Ultrasonics 93 (2019) 112–121

Contents lists available at ScienceDirect

Ultrasonics

journal homepage: www.elsevier.com/locate/ultras

Development of ultrasonic guided wave inspection methodology for steam generator tubes of prototype fast breeder reactor

M.M. Narayanan, Anish Kumar*, S. Thirunavukkarasu, C.K. Mukhopadhyay

Metallurgy and Materials Group, Indira Gandhi Center for Atomic Research, HBNI, Kalpakkam-603102, Tamil Nadu, India

ARTICLE INFO

Keywords:
Steam generator tubes
Axisymmetric guided wave mode
Long range propagation
FE simulation
Defect detection

ABSTRACT

An ultrasonic guided wave based methodology is developed for inspection of steam generator tubes of the prototype fast breeder reactor. To this aim, axisymmetric longitudinal mode (L(0,2)) at the frequency of 250 kHz is optimized using 3D-finite element simulation and experiments. The group velocity of mode L(0,2) at 250 kHz is found to be 5387 m/s. First, the long range propagation of the L(0,2) mode at 250 kHz is examined and the mode is found to propagate over a distance of 45.6 m with a sufficiently good SNR. Secondly, the detection of multiple defects such as circumferential, axial, partial-pinholes and tapered defects lying in the same line of sight is investigated using 3D-finite element simulation and the results obtained are validated experimentally for the first three cases. The sensitivities achieved are 0.23 mm depth (10%WT) for circumferential, axial and tapered defects and for partial-pinholes: 1 mm diameter and 1.38 mm depth (60%WT). Thirdly, 3D-FE simulations with ID and OD pinhole defects are performed which show that the ID and OD defects are detected by L(0,2) with a fairly similar sensitivity. Finally, study on the thermal expansion bend (with three successive bends) shows that the bend does not have much influence on the mode and the multiple circumferential defects considered in the bend are detected with good sensitivity.

1. Introduction

Heat exchanger tubes of a steam generator (SG) in fast reactors are of immense importance in nuclear power plants, as they carry water/steam inside the tubes surrounded by a hot flowing coolant. Any defect present in the tubes may lead to a serious accident causing heavy impact on the operation of a nuclear reactor. Therefore, a periodic assessment of integrity of the tubes using a suitable, reliable and rapid testing method is mandatory. One such application where the assessment of integrity of the tubes becomes important is the heat exchanger tubes of the steam generators of prototype fast breeder reactor (PFBR), a 500 MWe sodium cooled pool type reactor being commissioned at Kalpakkam, India. In PFBR, there are eight steam generators of 1.2 m diameter and the vertical height of 25 m each [1]. Each SG houses 547 steam generator tubes made of modified 9Cr-1Mo ferritic steel with tight control on chemistry to avoid scattering of mechanical and creep properties [2]. Each SG tube is of 23 m length with the outer diameter and the wall thickness of 17.2 mm and 2.3 mm, respectively. The SG tubes are welded to tube-to-tubesheet at the top and bottom of each SG and they are provided with a bend of 375 mm radius, to accommodate differential thermal expansion. The SGs are mounted vertically and are of counter-flow type with sodium entering shell side through a single sodium inlet nozzle at the top while water enters inside the heat exchanger tubes through the tube-to-tubesheet at the bottom and leaves as steam through steam outlet at the top [3].

If any leakage occurs in an SG tube of PFBR, sodium and high-pressure water/steam can react exothermically leading to the evolution of hydrogen, corrosive products and intense local heat. This may cause huge damage to the surrounding tubes and disrupt the smooth operation of the reactor. The possible cause of defects in the SG tubes are stress-corrosion cracks, pitting corrosion, erosion, arc strikes and spatter on the tube during welding, porosities in the weld and mechanical damage [4].Therefore, it is important to ensure the reliability of sodium-water/steam boundaries using a suitable non-destructing testing (NDT) method time-to-time. NDT methods used for the examination of heat exchanger tubes are eddy current testing, ultrasonic testing, visual testing and helium and hydro leak testing [5–7]. For in-service inspection of SG tubes of PFBR, remote field eddy current technique (RFEC) is proposed [8,9]. It requires the insertion of the RFEC probe into the tube all along the length of 23 m of the tube and hence, is very time consuming. Besides, RFECT is influenced by misalignment of coils, probe wobble, welds, permeability variations, and residual stresses and bends [10]. The technique is of low sensitivity as well. To circumvent the difficulties, ultrasonic guided wave based

* Corresponding author.
E-mail address: anish@igcar.gov.in (A. Kumar).

https://doi.org/10.1016/j.ultras.2018.11.003
Received 24 May 2018; Received in revised form 14 October 2018; Accepted 9 November 2018
Available online 10 November 2018
0041-624X/

inspection methodology has been developed for rapid inspection of the whole SG tube from one end without having to insert and guide a probe all along the length of the tube.

There is a considerable amount of literature available on the subject of ultrasonic guided wave propagation and detection of various flaws in pipes and tubes [11–29]. Generation of ultrasonic guided waves requires an ultrasonic transducer to be placed at a point for obtaining the complete information of healthiness of the structure in question. Unlike bulk waves (longitudinal and shear), there are many guided wave modes with different mode shapes at a given frequency in plates and pipes and they are, in general, dispersive (phase velocity is a function of frequency). This can make guided wave based inspection very complex and hence a suitable guided wave mode, instrumentation and signal processing must be chosen judiciously for a given application. This has led to many studies on optimization of modes [11].

The main application of long range ultrasonic guided wave testing is to pipes and tubes. The use of low frequency ultrasonic guided waves propagating along the tube wall for testing has become very attractive because of their nearly uniform stress throughout the wall thickness, less dispersion and less attenuation. The use of low frequency guided modes does not preclude the possibility of achieving the sensitivity required. In fact, such low frequency guided modes can detect defects whose depths are much smaller than the wavelength of a particular mode launched [12]. For instance, the use of axisymmetric longitudinal modes (L(0,m)) and torsional modes (T(0,m))at low frequencies (50 kHz-100 kHz) in tubes for detection of small defects and a long range propagation is prevalent in literature [13]. However, the modes exhibit different sensitivity to a given defect. L(0,m) modes can be easily excited using direct coupling of an ultrasonic transducer to the end of a tube [14,15], ring transducers wrapped over the tube [16], wedge transducers [17], comb transducers [18], EMATs [19] and magnetostriction [20]. T(0,m) modes can be excited by ring transducers wrapped over the circumference of the tube, EMATs [21]and magnetostrictive methods as well.

It is seen in the literature that L(0,n) and T(0,1) modes are widely used for detection of circumferential and axial cracks for various applications with the reflectivity obtained as a function of the dimensions of the defects [22–27]. It is seen that for long range testing of pipes either low frequency longitudinal (L(0,m)) or torsional modes (T(0,m)) have been used. For instance, Liu et al. [28] used T(0,1) mode at 50 kHz in a pipe of length 7.4 m, to detect a longitudinal defect. There were four end reflections, shown in the paper, amounting to the propagation distance of 58.92 m.

The defects that have been dealt with are mostly circumferential or axial and a very few studies have been reported on detection of pinholes and tapered defects. For instance, Lovstad et al. [29] have studied the reflection of T(0,1) mode from circular holes placed axially, circumferentially and at various angles using FE models and found the influence of separation distance of holes on the reflection coefficient. Tapered defects (axi-symmetric) have been studied as well by Carandente et al. [30] using T(0,1) mode. The defects considered in studies have been on the outside of pipes and no inside defect has been considered even in numerical simulations. The present study aims at the detection of multiple axial and circumferential defects, pinholes and tapered defects using a single mode.

Another major issue associated with adopting the guided wave technique for the SG tubes is the detection of flaws in the expansion bend regions. Several studies have been reported on the guided wave propagation in bent tubes. Heinlein et al. [31] studied the areas of detectability in a bend and reported that areas of low detectability were on the intrados while the areas of high detectability were close to extrados. Further, it was also reported that reflected amplitude of T(0,1) from circumferential cracks in the bend varies roughly with the square of the Von-Mises stress at the location of the defect. Jing Ni et al. [32] studied the propagation of L(0,2) across multiple bends and reported that the characteristics of propagation and the detection sensitivity vary from one bend to another in multiple bends. It is seen that the wave propagation in bends is complicated by mode conversion and distortion and thus a challenging problem.

The present paper deals with development of ultrasonic guided wave based methodology for a critical application of inspection of steam generator tubes for a fast breeder nuclear reactor, which has not been reported so far. A comprehensive study using both FE simulation and experiment has been performed to evaluate the sensitivity of the technique for detection of defects of various geometries. The requirement includes propagation of guided waves for intermediate range (~25 m) and defect detection with the required high sensitivity even in the presence of an expansion bend.

The objective of the study is fourfold, namely:

(i) Optimization of a guided wave mode for a long range propagation of 46 m (up and down travelling distance of the guided waves)

(ii) Detection of 10%WT deep circumferential, 10%WT deep axial defects, 2.3 mm diameter through-pinholes and 10%WT deep (max.), 15 mm length and 27 mm circumferential tapered defects

(iii) Detection of flaws in thermal expansion bends

(iv) Finally, the design and the development of a magnetostriction based guided wave sensor for generating the optimized guided wave mode which will be presented in our future publication.

The paper is organized as the following categories: (1) introduction, (2) theory, (3) the optimization of an ultrasonic guided wave mode using FE simulation, (4) experimental and specimen details and the details of FE models with multiple defects, (5) results and discussions: (a) experimental results for a 1 m long tube and FE result validation, (b) experimental long range propagation study, (c) validation of FE results obtained for multiple defects with that of experiments and FE results for the case of tapered defects, (d) comparison of FE simulations results for ID and OD pinhole defects, (6) experimental results for the multiple circumferential defects in a thermal expansion bend region of an SG tube and (7) summary.

1.1. Theory

Ultrasonic guided waves are formed between two boundaries by superposition of multiple reflections of shear and compressional waves between boundaries. The propagation of ultrasonic waves in a solid is governed by Navier's equation of motion [33], as shown in Eq. (1):

$$(\lambda + 2\mu)\nabla\nabla.\,\bar{U} - \mu\nabla \times \nabla \times \bar{U} = \rho\frac{\partial^2\bar{U}}{\partial t^2} \tag{1}$$

where, λ and μ are Lamé constants, $\bar{U}$ is the density of the solid and Ū is the displacement vector. When Navier's equation is solved in an infinitely long, homogeneous and isotropic hollow cylinder with traction free boundary conditions at the inner radius and the outer radius, it yields three different families of guided waves. The three families are termed the longitudinal (L(0,m)), torsional (T(0,m)) and flexural (F(n,m)) modes, where 'n' is the circumferential order and 'm' is the mode number. Within each family there are infinite numbers of modes with respective phase velocities. These modes are entirely determined by material properties, inner and outer radii of the tube and the frequency-wall thickness (fd) product. The zero order (n = 0) longitudinal and torsional modes are axisymmetric. L(0,m) modes have fields such as displacement and stresses as functions of axial (z) and radial (r) coordinates and independent of the angular coordinate θ. T(0,m) modes have the displacement field across the cross-section of the cylinder as a function of angular coordinate alone. All these modes can be visualized using dispersion curves plotted between phase velocity and frequency. Every point on the dispersion curves represents a valid mode that can exist in a tube.

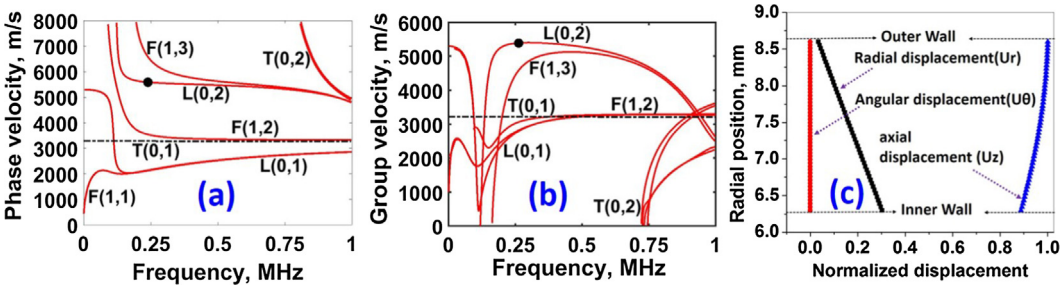

Fig. 1. (a) Phase velocity dispersion curves and (b) group velocity dispersion curves for SG tubes of PFBR, made of mod. 9Cr-1Mo ferritic steel with the inner diameter of 12.6 mm and the wall thickness of 2.3 mm and (c) mode shape of L(0,2) at 250 kHz.

2. Mode selection through Disperse software and FE simulation

2.1. Guided mode properties and mode selection using Disperse software

The SG tubes of PFBR are made of modified 9Cr-1Mo ferritic steel with the density of 7800 kg/m^3, Young's modulus of 220 GPa, the Poisson ratio of 0.2805, the longitudinal wave velocity of 6008 m/s and the shear wave velocity of 3319 m/s [34]. The inner and outer diameters of the tube are 12.6 mm and 17.2 mm, respectively and the wall thickness is 2.3 mm. With the inner radius, wall thickness and the elastic properties of the material of the tube, the phase velocity and the group velocity dispersion curves were obtained using Disperse software [35], developed at Imperial College. Fig. 1a and b show the phase velocity and the group velocity dispersion curves. It can be seen in Fig. 1a that F(1,2) and L(0,2) are nearly non-dispersive in the range of frequencies: 250 kHz–1 MHz and 200 kHz–650 kHz, respectively. The cut-off frequency of L(0,2) is around 150 kHz. From ~150 kHz to ~200 kHz, L(0,2) mode is highly dispersive. F(1,3), F(1,1)/L(0,1) in this frequency range are also dispersive and hence are discounted with. Further, T(0,2) is also dispersive. It can be seen in literature that either L(0,2) or T(0,1) mode is used for long range inspection. Between T(0,1) and L(0,2), L(0,2) at 250 kHz has been chosen for the following reasons: the highest group velocity, good separation from neighboring modes, fairly uniform axial stresses indicating fairly equal sensitivity and easy excitability using ultrasonic transducers and magnetostrictive principles. Above all, only accessibility for actual testing is from the inside of the tube whose inner area of cross-section is ~125 mm^2.

Owing to this constraint, magnetostrictive methods have been chosen for guided wave generation. Both L(0,2) and T(0,1) modes can be generated using magnetostriction methods. But given the above constraint of space, a magnetostrictive transducer generating L(0,2) is easier to fabricate and hence L(0,2) mode has been chosen. L(0,2) modes at higher frequencies in the range 250 kHz up to 650 kHz could be chosen for better sensitivity and resolution but there are two disadvantages. First, higher attenuation for higher frequencies is not desirable for long range propagation. Secondly, high frequencies exhibit reduced skin depth and consequently the effective volume of the distribution of magnetostrictive forces will be very low. This will result in inefficient generation of the wave mode. Thus, a wave frequency of 250 kHz has been selected from the perspective of lower attenuation and magnetostriction. The markers in the figures indicate the L(0,2) mode at the frequency of 250 kHz. The group velocity of this mode is 5380 m/s. The mode shape of the normalized radial and axial displacement components is shown in Fig. 1c. The axial displacement is fairly uniform across the wall thickness while the angular displacement component is zero. Further, the axial stress across a defect will be uniform indicating equal sensitivity. The dispersion curves are theoretically possible solutions (modes) but their excitability should be ascertained. To this end, FE simulation has been performed.

2.2. Finite element simulation

Ultrasonic wave propagation problems are solved using both implicit and explicit methods. In the present study, the finite element simulation software ABAQUS was used to simulate the wave propagation utilizing explicit time domain algorithm [36]. This algorithm is conditionally stable and the time step has to be smaller than the critical time step [37]. For the present study, a 3D-finite element model was developed to simulate L(0,2) mode propagation in a 1.0 m long steam generator tube. The model was assigned the elastic properties, as given in Section 2.1. The spatial step was chosen as 1/30th of the wavelength (13 mm) of the shear wave at 250 kHz which is 0.45 mm and the time step of 1e-8s was chosen based on time required for the longitudinal wave to travel the spatial step of 0.45 mm. Both steps were seen to be sufficient to meet the convergence criterion. The wavelength of the mode L(0,2) at 250 kHz is 21.5 mm and hence, there are nearly 50 elements across the wavelength. The number of through-thickness elements was chosen to be 6. The geometry was meshed with six-node linear triangular prism elements (C3D6). To excite L(0,2) at 250 kHz, the excitation pulse was applied axi-symmetrically on the end face of the tube, as an axial displacement (Uz) with a five cycle Hanning windowed toneburst of 250 kHz center frequency. Fig. 2a and b show the excitation and reception location at one end of the tube and the mesh used in the simulation, respectively. Fig. 2c shows the five-cycle windowed toned burst. The FE simulation was carried out with the above parameters which clearly showed the generation and the propagation of L(0,2) mode at 250 kHz.

Fig. 3a shows the averaged axial time domain signal picked up at

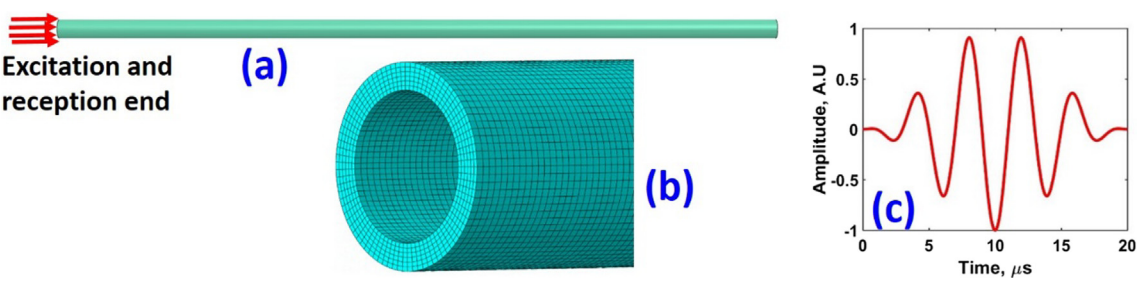

Fig. 2. (a) Excitation along z-axis, (b) mesh and (c) excitation signal used in FE simulation.

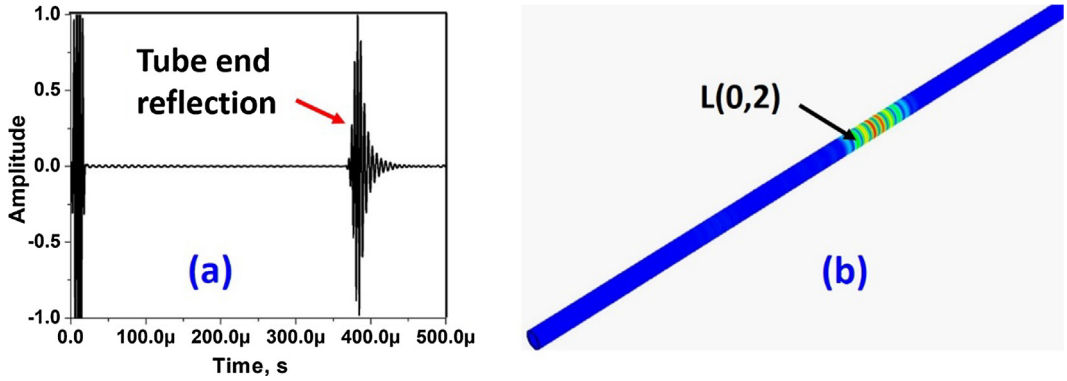

Fig. 3. (a) Averaged time signal (Uz) obtained from the excitation end and (b) L(0,2) obtained from the FE simulation at 65 μs.

the excitation end and the screenshot of the propagation of L(0,2) mode at 65 μs is shown in Fig. 3b. The group velocity observed was 5367 m/s. Further, the variation of Uz from OD to ID was found to be very small. This result is in complete agreement with that obtained from Disperse software. The radial displacement was observed to be very small and it was not considered because the ultrasonic transducer used in the experiment works on the longitudinal mode and it will be insensitive to radial components.

2.3. Experimental

The schematic of the experimental set-up is shown in Fig. 4. To generate the L(0,2) mode, an ultrasonic transducer (M/s. Panametrics) of centre frequency 250 kHz and the diameter of 40 mm was directly coupled to the one end of the tube and excited by a high power pulser-receiver (Ritec rpr-4000), using a 5-cycled toneburst. The signals received from the end of the tube were transferred to the oscilloscope through the pulser-receiver. The signals were sampled at 2.5 MHz and averaged 16 times and stored as ASCII data for post-processing. All the experiments in the study were carried out along the same lines. As the mode is axisymmetric, the symmetric coupling of an ultrasonic transducer on the end face efficiently generates L(0,2). But this way of generation will be efficient only when the transducer axis coincides with the axis of the tube.

2.4. Specimen details & experimental parameters

A tube of 1 m length without any defect was used to validate the propagation of L(0,2) mode, as indicated by FE simulation. A 3.8 m long tube was used for determining the long-range propagation of the mode. The four types of defects that can possibly occur in heat exchanger tubes are circumferential and axial defects due to stress-corrosion cracking [38,39], pinholes due to pitting corrosion [40] and tapered defects due to fretting [41]. The dimensions of the defects are chosen in accordance with our requirement. First three types of defects have been machined using EDM technique and tapered defects have been studied using FE simulation alone. All the defects are chosen to lie along the same line to study shadowing effect, if any. Fig. 5 a and b show the respective defects with their inter-separation in straight tubes and a 3 m long thermal expansion bend of an SG tube with circumferential

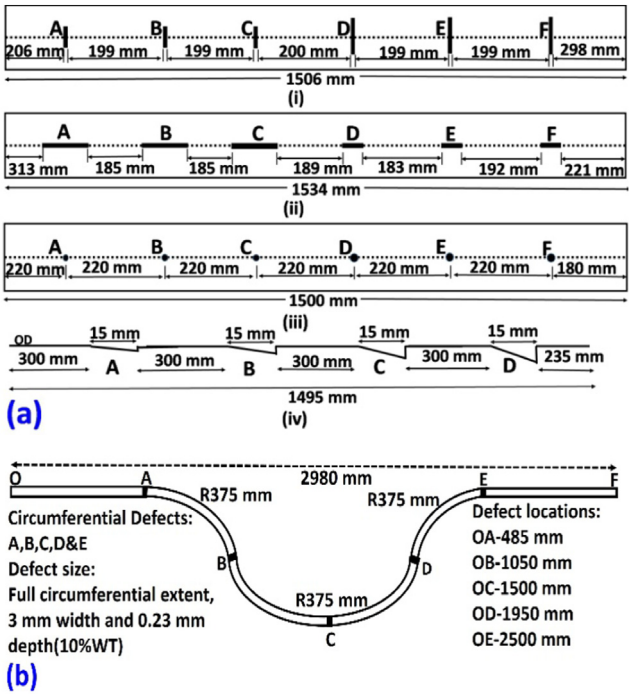

Fig. 5. a: (i) Circumferential defects, (ii) axial defects, (iii) pin-holes and (iv) tapered defects and (b) schematic of a thermal expansion bend with five circumferential defects at different locations.

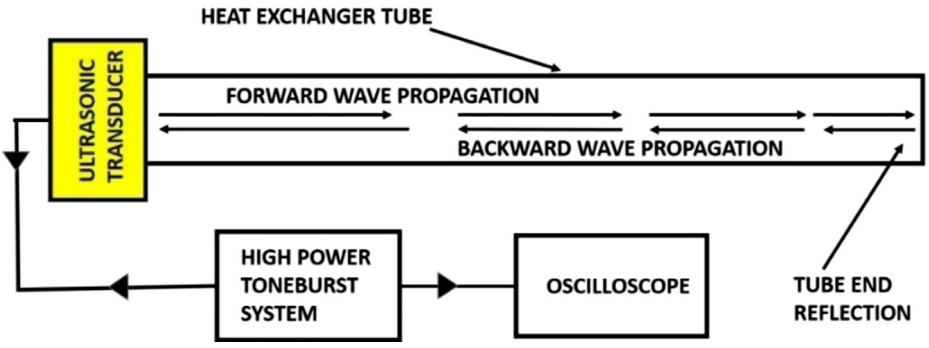

Fig. 4. Schematic of the experimental set-up.

Table 1
Type of defects, locations and their dimensions.

S.no.	Defect label	Circumferential defects (1 mm width)			Axial defect (1 mm width)			Pinhole defects (partial)			Tapered defects (27 mm CE, 15 mm AL)		Circumferential defects in thermal expansion bend (CE 360 deg, width 3 mm)location from left end to start of the defect (mm), Fig. 10
		CE, mm	D, mm	OL, mm	AL, mm	D, mm	OL, mm	Dia. mm	D, mm	OL, mm	D, mm	OL, mm	
1	A	7	0.23	206	15	0.69	313	1	0.92	220	0.23	300	485
2	B	7	0.46	406	15	0.46	513	1	1.38	440	0.46	615	1050
3	C	7	0.69	606	15	0.23	713	1	1.84	660	0.69	930	1500
4	D	15	0.23	807	7	0.69	917	2	0.46	880	0.92	1245	1950
5	E	15	0.46	1007	7	0.46	1107	2	0.92	1100	———	———	2500
6	F	15	0.69	1207	7	0.23	1306	2	1.38	1320	———	———	———

CE: Circumferential extent, D: depths of axial, circumferential, pinhole and tapered defects, AL: axial length of axial and tapered defects, Dia.: diameters of pinholes and OL: locations of the respective defects w.r.t. the left ends of the tubes. All the defects were made on the outer dia.(OD) of the tubes.

defects, respectively. The bent tube has three bends with each having the radius of curvature of 375 mm. Table 1 shows the type of the defect, size and the respective distances measured from the left ends of the tubes. Experiments were conducted on all the specimens, as stated in Section 2.3. In all the cases, different excitation voltage and amplification gain values were used to ensure data acquisition with high sensitivity. The bandpass filter of 50 kHz-1.6 MHz and the averaging of 16 were used throughout. The experimental parameters used were 274 V excitation voltage and 30 dB gain, 520 V and 32.8 dB and 575 V and 42.8 dB gain for the cases of Fig. 5a(i–iii) and 78 V and 34 dB for the case of the bent tube.

2.5. Finite element simulation for tubes with defects

FE simulation studies were carried out in 1.5 m long tubes with six OD circumferential defects, six OD axial defects, six OD pinholes of various dimensions and four tapered defects, as listed in Table 1. Besides, FE models with ID and OD partial-pinholes in 750 mm long tubes were also considered. All the FE programs were run in two steps, namely the excitation step and the wave propagation step in ABAQUS/Explicit solver.

3. Results and discussion

3.1. Experimental results for a 1 m long tube

Fig. 6 shows the experimental time signal obtained in the tube of 1 m length. The experimental signal resembles closely to that obtained from simulation (Fig. 3a). The times of flight of the FE and the experimental signals agree well. To ascertain the modes, time–frequency plots were made using the reassigned short time Fourier transform and the dispersion curves were overlaid on the plots [42]. Fig. 7a and b show the dispersion curves overlaid on the reassigned group velocity-frequency plots for the experimental and FE simulation signals, as shown in Fig. 6 and Fig. 3a, respectively and they correlate well. It can be seen that the modes present are only L(0,2) modes covering the frequency range of 100 kHz–300 kHz. The lower end of the bandwidth of 200 kHz comprises of frequency components that propagate slower than the higher frequency components. This will lead to a change in the group velocity. The group velocity obtained in experiments and FE models are 5387 m/s and 5367 m/s, respectively and that obtained using Disperse software is 5380 m/s. There is a good agreement between the observed group velocity and that provided by Disperse software. The relative errors in the group velocity w.r.t. 5380 m/s are about 0.1% and 0.2% for the experimental and FE predicted group velocity, respectively.

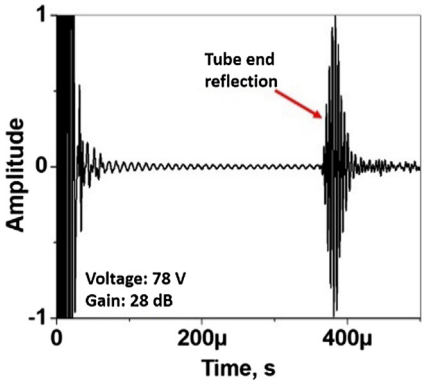

Fig. 6. Experimental signal obtained from the end of the tube of 1 m length.

3.2. Long range propagation of L(0,2) mode at 250 kHz in a 3.8 m long tube

The experimental time signal and the corresponding spectrogram for a 3.8 m long tube are shown in Fig. 8a and b, respectively. Fig. 8a shows that there are six multiple reflections which amount to the propagation distance of 45.6 m against the required 46 m. The maximum distance of propagation was limited by the pulse repetition frequency of the equipment used. It can be observed that though dispersion is present, its effect is not very severe in the long range, but it may have a consequence on the resolution of closely spaced defects. Fig. 8b clearly shows that the frequency components at the lower end of the bandwidth separate out with time and trail the higher frequencies and eventually die out due to dispersion of frequencies lower than 250 kHz. The majority of the higher frequency components reach a distance of 45.6 m, as predicted by Fig. 7b.

Further, to examine L(0,2) at 250 kHz in comparison with nearby L(0,2) modes, experiments were also conducted with the frequencies of 180 kHz and 500 kHz. Fig. 8c shows the plot of maximum amplitudes obtained with 180 kHz, 250 kHz and 500 kHz. The average attenuations for 180 kHz, 250 kHz and 500 kHz are 0.56 dB/m, 0.72 dB/m and 1.01 dB/m, respectively. The highest attenuation is shown by 500 kHz followed by 250 kHz and 180 kHz. However, the modes generated for all three frequencies were able to propagate for the distance of 45.6 m. It was observed that the time duration of wavepackets with the center frequency of 180 kHz was large indicating a poor resolution. Further, the mode at 500 kHz centre frequency suffers serious mode conversions in presence of non-axisymmetric defects and exhibit highest attenuation. On these grounds, the L(0,2) mode at 250 kHz has been selected for all the study, discounting with the other frequencies. Further, the FE results indicate that U_θ component of the displacement is three orders lower than U_z. This means that L(0,2) mode gets reflected almost entirely without significant mode conversion losses. There could be additional loss if the ends of the tube are not cut exactly perpendicular to the tube axis. Hence, the attenuation calculated can be considered to be the upper bound. This assumption has also been used by Aristegui et al.

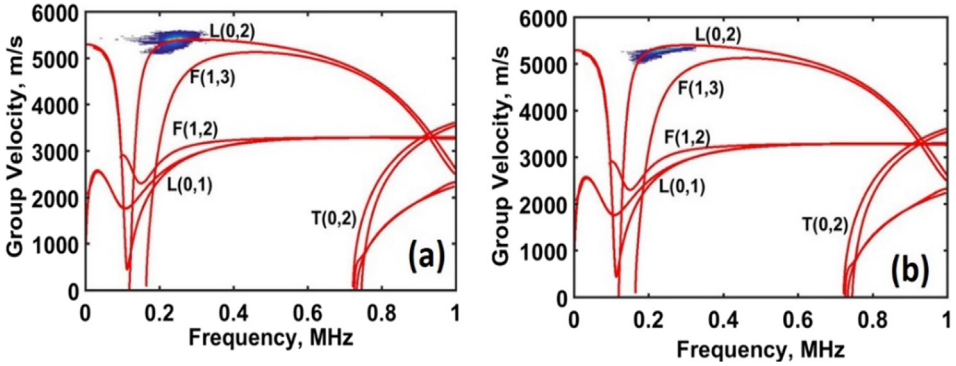

Fig. 7. Dispersion curves overlaid on spectrograms: (a) experimental signal (Fig. 6) and (b) FE simulation signal (Fig. 3a).

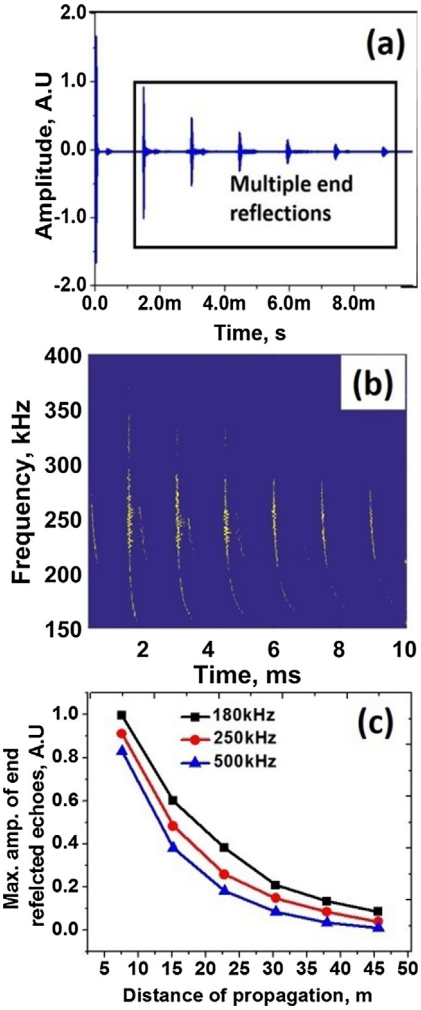

Fig. 8. (a) Experimental signal obtained on a 3.8 m long tube and (b) frequency versus time of propagation (c) Maximum amplitudes of end reflections obtained with 180 kHz, 250 kHz and 500 kHz.

[15]. The mode L(0,2) at 250 kHz has been found to be satisfactory in terms of ease in its excitability and a long range propagation and acceptable dispersion. However, the suitability of this mode for the application can be judged only based on its response to defects. The following sections discuss the defect detection capability of the L(0,2) mode at 250 kHz, to be specific multiple defects.

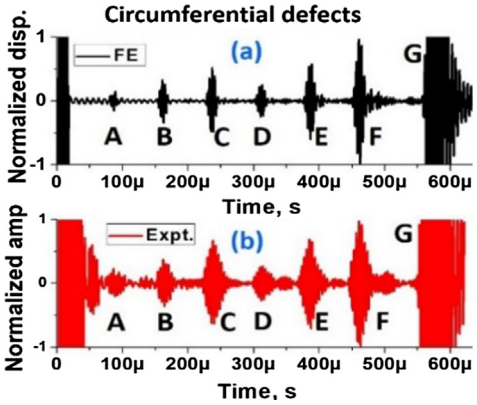

Fig. 9. Comparison of circumferential defect signals obtained using (a) FE and (b) experiment. **A-F** are defect labels, as in Table 1. **G**, the tube end reflection.

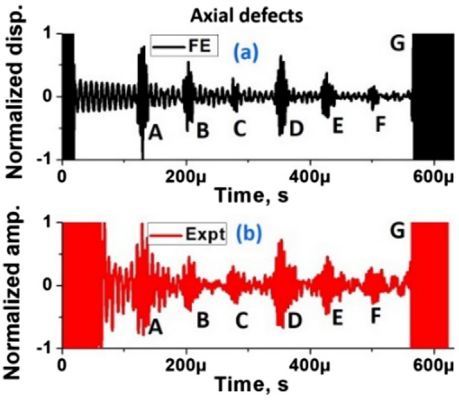

Fig. 10. Comparison of axial defect signals obtained using (a) FE and (b) experiment. **A-F** are defect labels, as in Table 1. **G**, the tube end reflection.

3.3. Circumferential defects, axial defects, partial pinholes and tapered defects

Figs. 9–11 show FE simulated and experimental time signals obtained for circumferential defects, axial defects and partial-pinholes, respectively. Fig. 12 shows the FE time signal for the case of non-axisymmetric tapered defects. Fig. 13a, c and e show the amplitudes of the individual defect signals in Figs. 9–11. The reasonable measure of the amplitudes and the corresponding times of flight were obtained by taking the envelope of the signals and then choosing the peak amplitudes and their corresponding times of flight. The experimental and FE amplitudes show good correlation for all the cases. In Figs. 9–11 the end reflections saturate, hence all the respective amplitudes were normalized w.r.t. the highest amplitude in each case. It can be observed that all

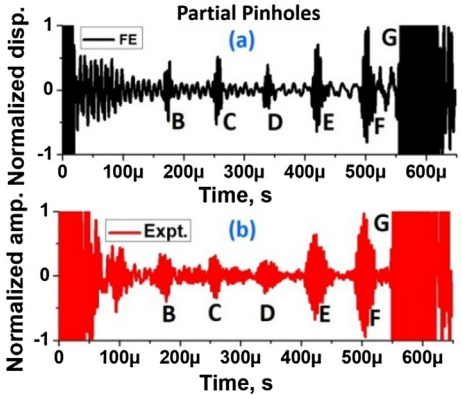

Fig. 11. Comparison of pinhole defect signals obtained using FE and experiment. **B-F** are defect labels, as in Table 1. **G**, the tube end reflection.

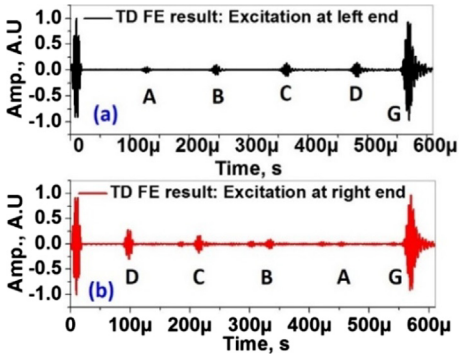

Fig. 12. FE Tapered defect (TD) signals for excitation at (a) left and (b) right ends. **A-D** are defect labels, as in Table 1. **G**, the tube end reflection.

six circumferential and axial defects were detected with good SNR. For the case of partial-pinholes, all but the 1 mm diameter and 0.92 mm deep pinhole were detected with good SNR. The SNR of the highest response in all three cases turn out to be approximately 21 dB. Fig. 13b, d and f show the difference in times of flight (a measure of error) observed in the FE and experimental defect signals in Figs. 9–11. They show a good agreement within the accuracy of max. 1.5 μs. It can be seen in Figs. 9–11, that the amplitudes increase or decrease in accordance with the size of the defect. The amplitudes corresponding to the circumferential defects (Fig. 13a) show an increasing linear response with depth and are also influenced by circumferential extent due to the increased area of interaction. The reflected amplitude should vary with width also. The reflected amplitudes for axial defects (Fig. 13c) show an increasing linear response with depth and are also influenced by axial length due to the interference happening between the signals reflected from the start and the end of the axial defect. Hence, it is always recommended to use two inspection frequencies [43] in the case of axial defects. For the case of pinholes, the reflected amplitudes (Fig. 13e) increase both with diameter and the depth.

Fig. 12 a and b show the FE time signals for non-axisymmetric tapered defects obtained by left excitation and right excitation of Fig. 5a (iv). The reflected amplitudes from left to right and vice-verse increase and decrease, respectively because of order of defects seen by L(0,2). The responses in the two cases are similar but for the multiple reflections between the tube end and defect D in Fig. 12b (seen between D&C, C&B and B&A). It can be seen that the flat part of a tapered defect is more effective in interaction than the tapered part. For instance, defect D when it is seen by L(0,2) mode from the right, it sees the flat of the defect first and hence, gives more reflected amplitude than when it sees the tapered part from the left. It is reported in the literature [30] that there will be separate reflections from the start and end of a taper. It is not noticed here because the linear dimension of the defect is smaller than the wavelength of L(0,2) (21.5 mm) and hence the reflections will merge to a single signal.

Fig. 14 shows the plot of reflected amplitudes from non-axisymmetric tapered defects for the right and left excitation. The reflected amplitudes increase non-linearly with the depth of the non-axisymmetric tapered defects. However, the circumferential and axial defects and the pinholes show a linear response with depth (Fig. 13). The amplitude profiles in Fig. 14 are not symmetric in both cases which may be due to different shape of the defects seen by L(0,2) when propagating from left to right and vice-versa. Fig. 15a shows the comparison of FE

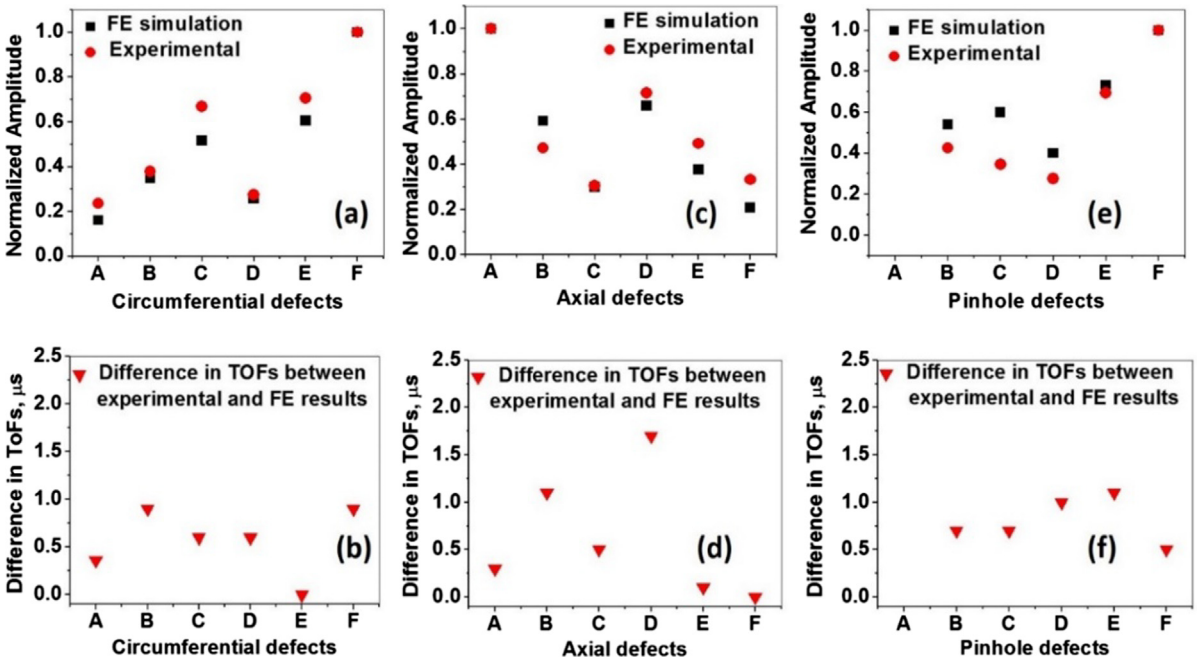

Fig. 13. Comparison of amplitudes and TOFs, respectively for FE and experimental time signals, respectively: (a and b) circumferential defects, (c and d) axial defects, and (e and f) partial pinholes, respectively. A-F represent defect labels, as given in Table 1.

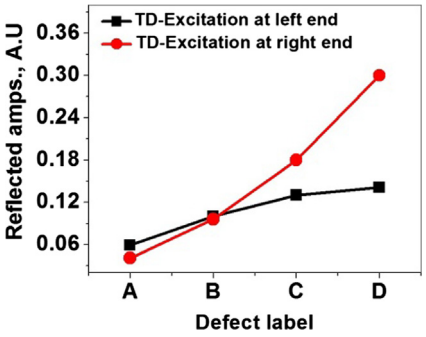

Fig. 14. Reflected amplitudes from tapered defects (TD) right and left excitation.

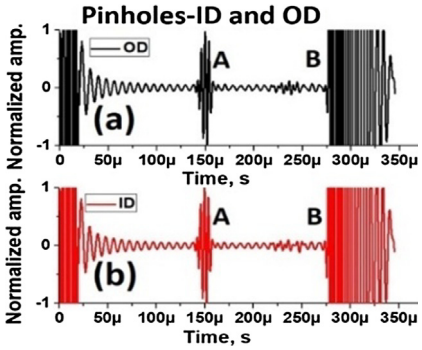

Fig. 16. Comparison of (a) ID and (b) OD pinhole signals obtained using FE simulations. **A** refers to the defect signal and **B,** the tube end reflection. The diameter and the depth of the pinhole are 1 mm and 1.38 mm, respectively.

reflected amplitudes for the tapered defect, circumferential defect, axial defect and partial-pinhole with all having the same 0.46 mm depth but with different percentages of cross-section. The response of the tapered flaw is the highest followed by the circumferential defects, axial defects and the pinhole for the same depth of 0.46 mm. It substantiates that the area presented by the defect to the mode L(0,2) governs the reflection. Fig. 15b shows the error in locating a defect for all four defect types. It can be seen that a defect can be located within the accuracy of max. 10 mm even when multiple defects are present. The maximum errors in locating a defect are for axial and tapered defects having larger axial extent due to the superposition of reflected signals arising from the start and the end of the defects.

The response of L(0,2) mode at 250 kHz to various defects such as circumferential, axial, pinhole and tapered defects has been studied. The response is found to be satisfactory in terms of the requirement for sensitivity (6 dB from noise level). For instance, the background noise level for experimental pinhole defect signals is in the range of ± 0.1 V in absolute terms and a 6 dB criterion is used for fixing the sensitivity which means a pinhole defect signal greater than ± 0.2 V will represent a defect signal. In the present case, the pinhole of dimensions: 1.38 mm (60%WT) depth and 1 mm diameter shows ~0.35 V and the pinhole of dimensions: 0.46 mm (20%WT) depth and 2 mm diameter shows ~0.25 V. The percentages of cross-section for the first and the second defects (mentioned here) are 1.38% and 0.85%, respectively assuming the equivalent reflecting areas (rectangular) for the curved surface. Hence, a pinhole with 1.38% cross-section has been considered for the sensitivity due to its smaller volume occupied by the defect than the 2 mm dia. pinhole. It can be seen that the reflected amplitude is governed more by the depth and less by the diameter of the pinhole because of the curved reflecting area. Further, to check if any mode conversion occurred during the interaction of L(0,2) mode with the defects U_r and U_θ components were recorded in addition to U_z in the FE simulations. The results show that there are indeed, mode conversions occurring due to the interaction of L(0,2) mode with the non-axisymmetric defects chosen in the study. This fact is reported in the literature that when a symmetric mode like L(0,2) is incident on a non-axisymmetric feature, there will be a mode conversion to F(1,3) and F (2,3) [44]. Since the ultrasonic transducer arrangement (symmetric system) used in the study can pick up only axial displacements, mode conversion to the angular and the radial displacements is not observed.

3.4. FE results for ID and OD pinhole defects

It is difficult to fabricate an ID defect. Hence, to study the response of an ID defect to L(0,2) mode at 250 kHz, FE simulations have been performed with both ID and OD pinholes. The defects were placed at 375 mm in 750 mm long tubes. Fig. 16 show the FE signals for the cases of ID and OD pinholes, respectively. It can be clearly observed in Fig. 16a and b that the ID and OD pinhole defects are obtained with the signals of similar amplitudes (normalized) due to the nearly uniform axial stress of L(0,2). Thus, it indicates that irrespective of the angular (θ) and through-thickness defect locations of a given defect at a particular z coordinate, the defect can be detected with similar SNR. The results were observed to be true for circumferential and axial defects as well.

3.5. Experimental results for circumferential defects in the thermal expansion bent section of the steam generator tube

It is a known fact that propagation of guided waves in bends is complicated by dispersion and mode conversions [45]. This can lead to a further complication when a defect is present in the bend. Hence, it can be very challenging or involved task to detect a defect in a bend region. Fig. 17 shows the experimental results obtained for a bent tube with five circumferential defects, as shown schematically in Fig. 5b. The labels A, B, C, D and E in the figure represent defect signals and the label F represents the end reflection. It can be observed that the

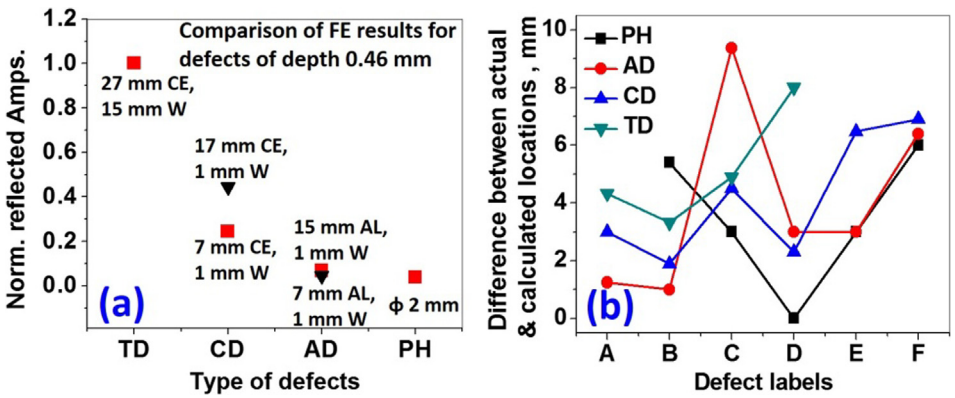

Fig. 15. (a) Comparison of FE amplitudes for a tapered defect (TD), circumferential defects (CD), axial defects (AD) and pinholes (PH) of the same 0.46 mm depth and (b) Error between FE estimated locations of the defects and the original locations of the defects Vs. defects. All the amplitudes are normalized w.r.t. to the amplitude of the tapered defect. CE: circumferential extent, AL: axial length, W: Width.

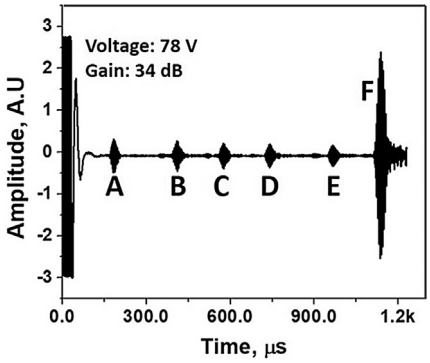

Fig. 17. Experimental signal obtained in a bent tube. **A-E** are circumferential defect labels, as in Fig. 5b (and the dimensions and the locations of which are given in Table 1) and they represent corresponding defect signals. **F**, the tube end reflection.

response of the defects in the bend to L(0,2) mode is good and the mode is able to propagate through the bend without much mode conversion and dispersion. Hence, it appears to be nearly straight from the perspective of the mode L(0,2). The circumferential defects considered were of the same size and this fact is also evidently brought out by the relative amplitudes of the defects **A-E**. It is reported in the literature that the reflected amplitudes strongly depend on the location of a defect in the bend. However, it can be observed that the reflected amplitudes do not vary much with the location of a defect in the three successive bends. The locations of the defects are accurate to within 10 mm.

4. Summary

In this paper, ultrasonic guided wave propagation and the detection of defects in steam generator tubes of PFBR have been presented systematically. The study is summarized as follows:

- An axisymmetric longitudinal mode L(0,2) was optimized at 250 kHz using finite element simulation and experiments. The group velocity of the mode was found to be 5387 m/s and the attenuation exhibited by the mode is 0.72 dB/m.
- The mode L(0,2) was examined for its long range propagation in a 3.8 m long tube and the maximum distance of propagation achieved was 45.6 m based on multiple reflections. The mode exhibited negligible dispersion whose consequence is not severe.
- The detection of multiple defects namely circumferential, axial and pinhole defects lying in the same line of sight was examined using FE simulation and experiments. The experimental and simulation results correlated well. Following are the smallest defects (considered in the study) detected:

(a) Circumferential defect: 0.23 mm (10%WT) depth, 7 mm circumferential extent and 1 mm width.
(b) Axial defect: 0.23 mm (10%WT) depth, 7 mm axial length and 1 mm width.
(c) Pinhole defect: 1.38 mm (60%WT) depth and 1 mm diameter.
(d) Tapered defect: 0.23 mm maximum depth (10%WT), 15 mm length and 27 mm circumferential extent.

- FE simulations for the cases of ID and OD pinhole defects were carried out. The responses of the defects to L(0,2) were observed to be similar.
- Finally, the influence of the thermal expansion bend on the L(0,2) and the detection of circumferential defects in the bend were studied. The thermal expansion bend presented negligible distortion to the mode and all the circumferential defects were detected with good sensitivity.

The mode L(0,2) meets all the requirement of long range propagation, detection of different defects in the straight section and in the bend in terms of sensitivity. It can be concluded that multiple defects lying even in the same line can be located fairly accurately. The results also indicate that one defect is not shadowed by another for the given inter-separations. Further, the defects considered in the study were very small and the technique can be expected to work even in real situations because of the two reasons. First, there are no features in the SG tube from start to end (23 m length) that can cause reflections and even the thermal expansion bend does not cause reflections of considerable amplitudes and mode conversions. Secondly, these tubes are supported by support plates (egg crate plates) which are not tightly clamped or acoustically coupled and hence, it can be said that the influence of the stress caused by the supports on L(0,2) will be negligible. Based on the outcome of the study, a magnetostrictive sensor has been designed to generate L(0,2) at 250 kHz and the results were observed to be quite similar to what has been discussed and this will be detailed in our next publication.

References

[1] T.K. Mitra, Aravinda Pai, Prabhat Kumar, Challenges in manufacture of PFBR steam generators, Energy Procedia 7 (2011) 317–322.
[2] Baldev Raj, B.K. Choudhary, R.K. Singh Raman, Mechanical properties and non-destructive examination of chromium-molybdenum ferritic steels for steam generator application, Pressure Vessels Piping 81 (2004) 521–534.
[3] R. Srinivasan, P. Chellapandi, C. Jebaraj, Structural design approach of steam generator made of modified 9Cr-1Mo for high temperature operation, Trans. Indian Inst. Metals 63 (2–3) (2010) 629–634.
[4] S. Thirunavukkarasu, B.P.C. Rao, G.K. Sharma, C. Viswa Chaitanya, T. Babu Rao, Jayakumar, Baldev Raj, Arvinda Pai, T.K. Mitra, Methodology for nondestructive assessment of integrity of steam generator shell welds, Int. J. Struct. Integrity 2 (2) (2011) 145–157.
[5] H.M. Sadek, NDE technologies for examination of heat exchangers and boiler tubes-principles, advantages and limitations, Insight 48 (2006) 181–183.
[6] R.M. Shriwardhankar, P.B. Patil, Mahesh Limaye, Development of helium leak testing system and procedure for testing welds of steam generator, Energy Procedia 7 (2011) 638–644.
[7] B.S. Yoon, S.H. Yang, Y.S. Kim, H.J. Lee, Steam Generator Tube Inspection of Nuclear Power Plants Using Ultrasonic Testing, Transactions of the Korean Nuclear Society, Korea, 2006.
[8] S. Thirunavukkarasu, B.P.C. Rao, T. Jayakumar, Baldev Raj, Techniques for processing remote field eddy current signals from bend regions of steam generator tubes of prototype fast breeder reactor, Annals of Nuclear Energy 38 (2011) 817–824.
[9] S. Vaidyanathan, S. Thirunavukkarasu, B.P.C. Rao, T. Jayakumar, P. Kalyanasundaram, Baldev Raj, Development of remote field eddy current technique for in-service inspection of ferromagnetic steam generator tubes, J. Non-destruct. Testing Evaluat. 4 (1) (2005) 26–30.
[10] Standard practice for in-situ examination of ferromagnetic heat-exchanger tubes using remote field testing, ASME Article 26 SE-2096, ASTM Section V 2010, 556–565.
[11] Ming-fang Zhenga, Chao Lua, Guo-zhu Chenb, Ping Men, Modelling three dimensional ultrasonic guided wave propagation and scattering in circular cylindrical structures using finite element approach, Physics Proceedia 22 (2011) 112–118.
[12] A. Tatarinov, Evgency N. Barkanov, E. Davydov, M. Mihovski, T- and L-types of long-range guided waves for defect detection, Non-destructive testing and Repair of pipelines, Engineering Materials, Springer International publishing, 2018, pp. 15–29.
[13] M.J.S. Lowe, P. Cawley, Long range guided wave inspection usage–current commercial capabilities and research directions, Technical report, Department of Mechanical Engineering, Imperial College, London, UK, 2006, pp. 1–40 https://www3.imperial.ac.uk/pls/portallive/docs/1/55745699.pdf.
[14] D.N. Alleyne, P. Cawley, The excitation of Lamb waves in pipes using dry-coupled piezoelectric transducers, J. Nondestruct. Evaluat. 15 (1) (1995) 11–20.
[15] C. Aristegui, M.J.S. Lowe, P. Cawely, Guided waves in fluid-filled pipes surrounded by different fluids, Ultrasonics 39 (2001) 367–375.
[16] P.S. Lowe, Ruth M. Sanderson, Nikolaos V. Boulgouris, Alex G. Haig, Wamadeva Balachandran, Inspection of cylindrical structures using the first longitudinal guided wave mode in isolation for higher flaw sensitivity, IEEE Sens. J. 16 (3) (2016) 706–714.
[17] Hyeon Jae Shin, L.Joseph Rose, Guided wave tuning principles for defect detection in tubing, J. Nondestruct. Evaluat. 17 (1998) 27–36.
[18] E. Thomas, R. Hay, Joseph L. Rose, Flexible PVDF comb transducers for excitation of axisymmetric guided waves in pipe, Sens. Actuat. A 100 (2002) 18–23.
[19] Xu Jiang, Yong Sun, Jinhai Zhou, Research on the lift-off effect of receiving longitudinal mode guided waves in pipes based on the Villari effect, Sensors 16 (9) (2016) 1–14 1529.
[20] A.M. Cong, X. Wu, C. Qian, A longitudinal mode electromagnetic acoustic transducer(EMAT) based on a permanent magnet chain for pipe inspection, Sensors 16 (5) (2016) 1–18.

[21] Samuel Hill, Steve Dixon, Sri Harsha, K. Reddy, Prabhu Rajagopal, Krishnan Balasubramaniam, A new electromagnetic acoustic transducer design for generating torsional guided wave modes for pipe inspections, 43rd Annual Review of Progress in Quantitative Nondestructive Evaluation, Atlanta, AIP Publishing, 2017.
[22] Yong-Moo Cheong, Dong-Hoon Lee, Hyun-Kyu Jung, Ultrasonic guided wave parameters for detection of axial cracks in feeder pipes of PHWR nuclear power plants, Ultrasonics 42 (2004) 883–888.
[23] J.L. Rose, J.J. Diriti, A. Pilarski, K. Rajana, F. Carr, A guided wave inspection for nuclear steam generator tubing, NDT&E Int. 27 (6) (1994) 307–310.
[24] M.J.S. Lowe, D.N. Alleyne, P. Cawley, Defect detection in pipes using guided waves, Ultrasonics 36 (1998) 147–154.
[25] B. Yoon, S. Yang, H. Lee, Y. Kim, Detection and mode identification of axial cracks in the steam generator tube of the nuclear power plant using ultrasonic guided wave, J. Nucl. Sci. Technol. 47 (8) (2010) 754–759.
[26] A. Demma, P. Cawley, M. Lowe, A.G. Roosenbrand, The reflection of the fundamental torsional mode from cracks and notches in pipes, J. Acoustic. Soc. America 114 (2) (2003) 611–625.
[27] M. Ratassepp, S. Flecher, M.J.S. Lowe, Scattering of the fundamental torsional mode at an axial crack in a pipe, J. Acoustic. Soc. America 127 (2) (2010) 730–740.
[28] Wu. Liu Zenghua, He Cunfu Bin, Yang Shiming, Wang Xiuyan, Detection of longitudinal defect in pipes using torsional modes, Chinese J. Mech. Eng. 19 (2006) 146–150.
[29] Anders Lovstad, Peter Cawley, The reflection of the fundamental torsional guided wave from multiple circular holes in pipes, NDT&E Int. 44 (2011) 553–562.
[30] R. Carandente, J. Ma, P. Cawley, The scattering of the fundamental torsional mode from axi-symmetric defects with varying depth profile, J. Acoustic. Soc. America 127 (6) (2010) 3440–3448.
[31] S. Heinlein, P. Cawley, T.K. Vogt, Reflection of Torsional T(0,1) waves from defects in pipe bends, NDT&E Int. 93 (2018) 57–63.
[32] Jing Ni, Shaoping Zhou, Pugen Zhang, Yong Li, Effect of pipe bend configuration on guided waves-based defects detection: an experimental study, J. Pressure Vessel Technol. 138 (2) (2015) pp. 021203–1 -021203-9.
[33] J.L. Rose, Ultrasonic guided waves in solid media, Cambridge University Press, USA, 2014.
[34] Anish kumar, Correlation of microstructure and mechanical properties with ultrasonic parameters in metallic materials, Ph.D. thesis, Indian Institute of Technology, Kharagpur, India, 2005.
[35] Disperse software, User's manual, Version 2.0 (2000).
[36] Mickael Brice Drozdz, Efficient finite element modelling of ultrasonic waves in elastic media, Ph.D. thesis, Imperial College of Science, University of London, UK, 2008.
[37] Abaqus Analysis User's Manual 6.10.
[38] F. Hasan, J. Iqbal, F. Ahmed, Stress-corrosion failure of high-pressure gas pipeline, Eng. Failure Anal. 14 (2007) 801–809.
[39] L.J. Berchmans, S. Muralidharan, N.S. Rangaswamy, S. Natrajan, V. Sivan, S. Venkatakrishna Iyer, Stress-corrosion cracking and hydrogen embrittlement susceptibility studies on modified 9Cr-1Mo steel weldments in acidic and neutral media, British Corrosion J. 31 (3) (1996) 223–226.
[40] J. Paul Guyer, An Introduction to Liquid Process Piping, Second ed., Guyer Partners, 2017.
[41] Joseph R. Davis, Stainless Steels, ASM Specialty Handbook, ASM International, 1994.
[42] Marc Niethammer, Laurence J. Jacobs, Time-frequency representation of Lamb waves using the reassigned spectrogram, J. Acoustic. Soc. America 107 (5) (2000) 19–24.
[43] A. Demma, Interaction of guided waves with discontinuities Ph.D. thesis, Imperial College of Science, University of London, UK, 2003.
[44] M.J.S. Lowe, D.N. Alleyne, P. Cawley, The mode conversion of a guided wave by a Part-circumferential notch in a pipe, J. Appl. Mech. 65 (1998) 649–656.
[45] H. Nishino, K. Yoshida, Hideo Cho, M. Takemoto, Propagation phenomena of wideband guided waves in a bent tube, Ultrasonics 44 (2006) 1139–1143.